lubricants

MDPI

Article

Study on the Lubricating Characteristics of Graphene Lubricants

Yi Dong [1], Biao Ma [1], Cenbo Xiong [1,*], Yong Liu [2] and Qin Zhao [1]

[1] School of Mechanical Engineering, Beijing Institute of Technology, Beijing 100081, China; dongyi0219@163.com (Y.D.); mabiao@bit.edu.cn (B.M.); yudewuhou@outlook.com (Q.Z.)
[2] School of Energy and Power Engineering, North University of China, Taiyuan 030051, China; yongliu_epe@nuc.edu.cn
* Correspondence: xiongcenbo@bit.edu.cn

Abstract: Graphene is considered a good lubricant additive. The lubricating properties of graphene lubricant at different concentrations and temperatures are studied via a four-ball friction and wear-testing machine. The results show that the coefficient of friction (COF) and wear scar diameter (WSD) of the steel ball with 0.035 wt% graphene lubricant decreased by 40.8% and 50.4%, respectively. Finally, through surface analysis, the following lubrication mechanism is proposed: as the added graphene particles can easily fill and cover the pores of the friction surface, the contact pressure of the rough peak is reduced, resulting in a lower COF and smoother surface. Although the COF increases with temperature, graphene lubricants still exhibit good lubrication effects.

Keywords: graphene lubricant; friction and wear properties; roughness; lubrication characteristics

1. Introduction

In mechanical systems, frictional components serve as integral parts of the execution process, and they directly affect the system performance. During the working process, friction components are often operated in harsh environments, such as high-temperature, high-speed, and high-pressure conditions. Consequently, they are inevitably accompanied by a large amount of frictional heat and energy loss. It should be noted that energy loss due to friction is one of the typical forms of global energy consumption; more exactly, about 1/3 of the world's primary energy comes from friction consumption, and almost 1/2 of the power of transportation equipment is consumed in friction [1]. Subsequently, the resulting wear is the main cause of mechanical equipment failure. Generally, there are four ways to reduce friction and wear, including optimizing the bearing structure, improving the working conditions, and developing new friction materials and better lubricants [2].

Lubricants are indispensable because of their unique and effective anti-friction effects, especially for oil-lubricated bearings. Since the base oil does not have integral properties that enable it to withstand different working environments, it must be mixed with additives to improve its working performance [3]. Accordingly, the research of lubricant additives is promising regarding improvements in the anti-friction and anti-wear properties of the base oil [4]. Additives are one or more compounds added into lubricants in order to improve their properties [5]. The reasonable use of additives is crucial to ensure the quality of lubricants. Recently, research on various types of additives has become an attractive area. Nano additives have emerged with the development of the atomic friction model [6]. Nanoparticles have a large specific surface area and are easily adsorbed on the contact surface. Since atoms in the same atomic layer are bound by covalent bonds, a single-layer structure is formed with high modulus and high strength, avoiding direct contact with the friction pair [7]. Several excellent studies about nano additives in lubricants are available, such as metal nanoparticles [6–9], carbon element nanoparticles [10,11], oxide nanoparticles [12,13], various inorganic compound nanoparticles [14,15], polymer nanoparticles [16,17] and composite nanoparticles [18,19], etc.

check for updates

Citation: Dong, Y.; Ma, B.; Xiong, C.; Liu, Y.; Zhao, Q. Study on the Lubricating Characteristics of Graphene Lubricants. *Lubricants* **2023**, *11*, 506. https://doi.org/10.3390/lubricants11120506

Received: 6 November 2023
Revised: 25 November 2023
Accepted: 27 November 2023
Published: 30 November 2023

Many researchers so far have focused on graphene additives. They have several advantages, such as the chemical structure of ultra-thin glass sheets, kinetic and physical properties, and a better fluid self-lubricating transmission performance [20]. However, the deficiency of dispersibility has hindered their development in lubricating oil. Ka et al. [21] explored the tribological properties of graphene as an oil additive. After thorough research work [22], graphene was found to be prone to agglomerating in acidic lubricating oil and found to be unstable in alkaline solvent [23,24]. As for the synthesis methods used for graphene lubricants, there are three strategies employed to improve their dispersion stability [25,26], namely physical modification, chemical structure modification and microstructure. Su et al. [27] observed the lubricated wear scar surface after adding 0.25% graphite nanoparticles to vegetable-based oil. Graphite nanoparticles can be stably adsorbed on the friction surface and form a physical adsorption film on it. Flakes are formed due to precipitation and agglomeration. Since the modification effect can significantly improve the dispersibility of graphene, CI et al. [28] prepared fluorinated reduced graphene oxide nanosheets using a gas fluorination method to improve the load-bearing capacity and wear resistance of lubricants. Lau et al. [29] investigated the suspension stability of GBC and GSF particles (0.05 wt%) dispersed in a low-viscosity polyol ester lubricating oil and their tribological performance. It should be noted that, although graphene lubricants have already been proposed and applied [30], graphene's aggregation and precipitation phenomena in different lubricants, as well as its mechanism of friction and wear, still need to be further studied.

In the extensive applications of bearings, especially in some important devices such as heavy-duty vehicles, trains and vessels, they require regular lubrication to maintain exceptional performance. A lower and more stable coefficient of friction (COF) can improve the working performance and efficiency of bearings. In addition, a lower wear rate can significantly extend the practical life of bearings and devices. In this work, the friction and wear characteristics of graphene lubricants with different concentrations and temperatures are experimentally explored. The lubrication and wear mechanism are further proposed to illuminate the tribochemical interaction between carbon surfaces. The results are expected to provide some basic knowledge for improving the design of nanoparticle applications in lubricants.

2. Lubricant Preparation

The graphene lubricants were prepared using a constant-temperature magnetic stirring ultrasonic method. The lubricant preparation process is shown in Figure 1. Based on our previous study [31], oleic acid and stearic acid were selected as the graphene modifier ①, and the corresponding ratio was 9:10. Firstly, the mixture of oleic acid–stearic acid was placed in a beaker and heated to 80 °C; secondly, the modifier was obtained after stirring the mixture for 30 min; thirdly, a certain amount of graphene powder was weighed to prepare graphene lubricants of different concentrations. Subsequently, the Class I base oil 500SN without additives was added to the beaker as the lubricating liquid, and heated to 80 °C in a water bath with a thermostatic magnetic stirrer; then, the weighed graphene flakes were added into the beaker, and the magnetic stirring was started at a speed of 1200 rpm. The modifier was then added into the beaker at a constant speed through a micropipette and stirred for 60 min. After that, the solution obtained above was slowly moved into the ultrasonic two-dimensional material stripper for ultrasonic treatment for 30 min. Finally, a homogeneously dispersed and stable graphene lubricant was obtained [31].

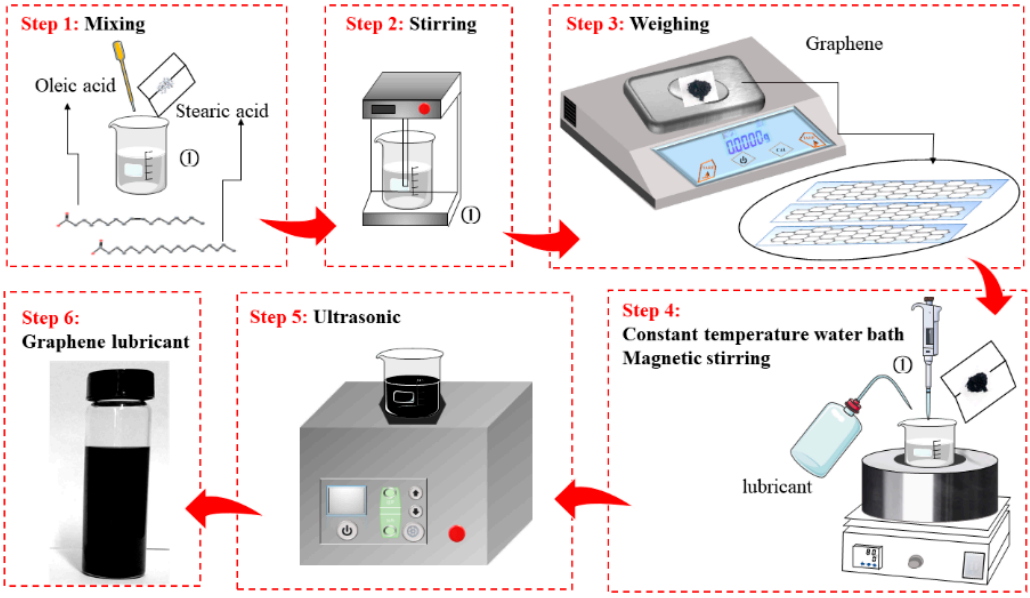

Figure 1. Flow chart of the overall preparation of graphene lubricant.

3. Friction and Wear Experiment

In this paper, we aim to explore the lubricating properties of graphene lubricants at different concentrations and temperatures experimentally. For this purpose, we would like to first introduce the experimental method and conditions that we used in this section.

3.1. Experimental Method

The experimental study was carried out on a lever-type four-ball friction and wear-testing machine (MR-S10G, Jinan Hengke Test Equipment Co., Ltd., Shandong, China, as shown in Figure 2), which is composed of a spindle drive system, a weight lever system, an oil box and a heater, a friction force measurement system, an electrical control system, a strong current system, etc., all of which are installed on the frame with the base as the main body. The spindle drive system is responsible for transmitting the rotational speed. A lever system is used to adjust the applied load. In addition, a measurement system is used to collect the coefficient of friction (COF). The COF is inversely proportional to the axial test force and proportional to the friction torque value. The obtained instantaneous COF is used to characterize the change in the whole experimental process, and the average COF is used to compare and analyze the globe friction characteristics under different conditions. The friction test was conducted using ASTM D5183-95 (1999) standard, from SH/T0762-2005.

The friction samples were four steel balls with a diameter of 12.7 mm. During the test, three steel balls were clamped in 10 mL of running-in oil; the other one was used as the upper steel ball to make three-point contact with the three steel balls, as shown in Figure 2. In this study, a long grinding test was carried out; the spindle speed was 1200 r/min, the test time was 60 min, and the oil pool was lubricated. Before the test, the required lubricating oil was sonicated in an ultrasonic machine for 30 min to ensure a good dispersion of the graphene in the base oil. After the test, petroleum ether was used to clean the test steel ball several times, and place it in a cool place to air dry. After the friction test, the surface morphology was observed via a scanning electron microscope (SEM), and the wear scar WSD of the worn surface could be obtained to evaluate the lubricating effect of the lubricant.

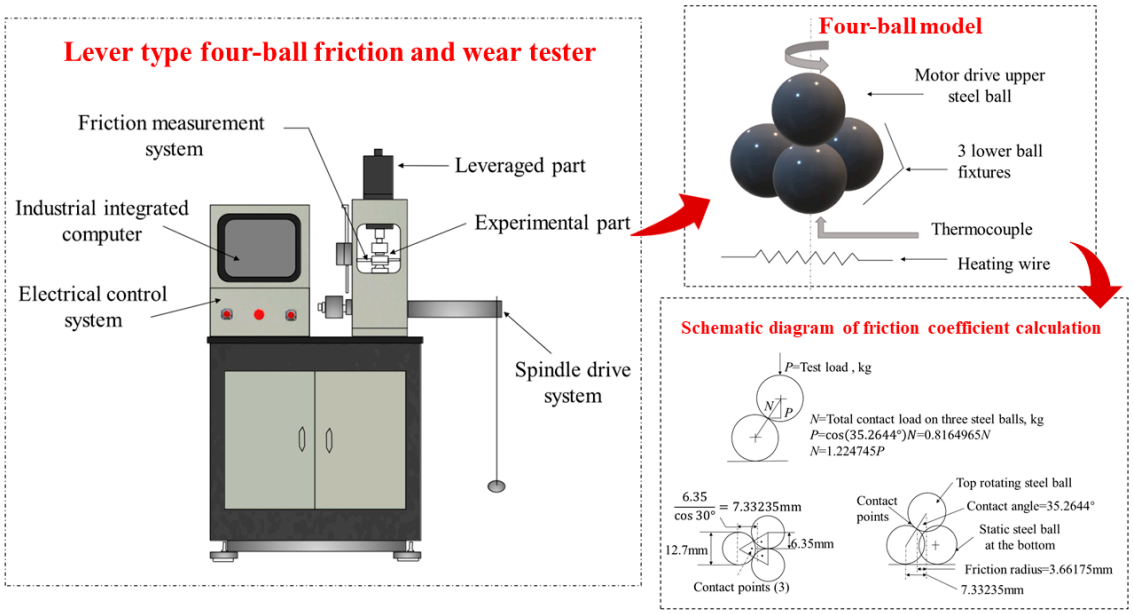

Figure 2. Structure and principle diagram of lever type-four-ball friction and wear testing machine.

3.2. Experimental Conditions

In this test, a 60 min long grinding test is carried out under the lubricated status. The specific experimental conditions are presented in Table 1. Since the effects of temperature and concentration are concerned in this study, four different temperature values and five different concentration values are chosen to compare the results. There are 20 groups of experiments, each with new steel balls. In addition, each experiment is repeated three times. Before the test, the graphene lubricant is sonicated in an ultrasonic machine for 30 min to ensure a good dispersion effect. After the test, the tested steel balls are cleaned several times with the petroleum ether and then dried in the shade.

Table 1. Experimental conditions of friction and wear tests.

Factors	Values
Load/N	392
Rotating speed/rpm	1200
Temperature/°C	25, 100, 150, 200
Concentration/wt%	0, 0.030, 0.035, 0.040, 0.050

4. Results and Discussion

In order to study the tribological behavior of the friction pair within lubricants, friction experiments were carried out under the same load of 392 N. In this section, the COF, surface morphology and 3D topography of the balls were tested to reveal the effects of temperature and concentration.

4.1. Tribological Characteristics

Figure 3 shows a set of typical COFs under different temperature and concentration conditions in one testing cycle. It can be observed that the COF curves display a running-in stage at the beginning of the test, which lasts about 1000 s. The COF in pure oil is almost higher than all of the other concentrations, except for the running-in stage in Figure 3d. During the running-in stage, the COF dramatically increases, decreases or fluctuates with time due to the change in friction surface topography. After the running-in stage, the COF becomes relatively stable. Since the variation trends of COF in one testing cycle may lead to incorrect conclusions, it is hard to tell the effects of concentration on the COF under

different temperature conditions. In order to obtain more reliable data and reduce the occasionality, the experiments are repeated for three times.

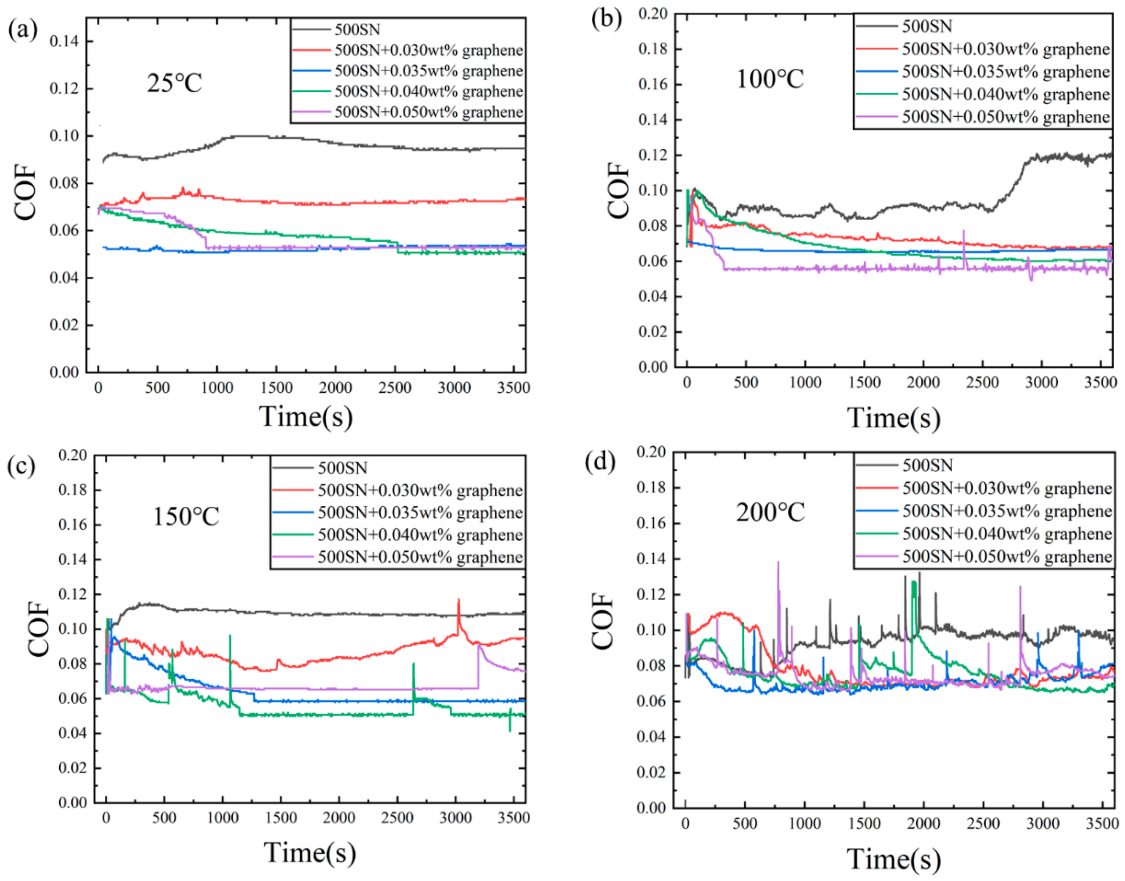

Figure 3. Instantaneous COF with different concentrations and temperatures:(**a**) 25 °C, (**b**) 100 °C, (**c**) 150 °C, (**d**) 200 °C.

Even though the COF undergoes fluctuations during some of the tests, it is stable most of the time. According to some relevant references, the average COF is commonly used to interpret the friction characteristics [6,32,33]. Therefore, the average COF for the whole run is also adopted here to show the effects of temperature and concentration. In Table 2, the time-average values of the COF during three tests are listed in the columns Test 1, Test 2 and Test 3. $\overline{f}$ is the mean value of the time-average COFs and σ denotes the standard deviation of the time-average COFs. The standard deviation of the test results is located in the range of 0.0003 to 0.0065 under 20 groups of working conditions. In this way, it is sufficient to prove the reproducibility of the experiment.

Figure 4 shows the mean COFs and the error bars under different temperature and concentration conditions. In terms of graphene concentration, it can be seen that not only are the mean COFs of the pure oil much higher than those of the graphene lubricants, but also their standard deviations are much larger than those of the graphene lubricants. It means that graphene lubricants make the average COF more stable than the pure oil. With the given temperature, the general trend is that, when the graphene concentration increases, the mean COF firstly decreases rapidly and then increases slowly. When the temperature is 25 °C, 0.035 wt% graphene lubricant has the lowest mean COF of 0.05170, which is 40.8% lower than the pure lubricant. In terms of temperature, the mean COF generally grows as the temperature increases. With a higher concentration of 0.035 wt% to 0.05 wt% and a higher temperature of 150 °C and 200 °C, the mean COFs are very close to each other.

Table 2. The average COF values of repeated experiments.

Temperature (°C)	Concentrations (wt%)	Test 1	Test 2	Test 3	$\bar{f}$	σ
25	0	0.08007	0.09248	0.08931	0.08729	0.00645
	0.03	0.06319	0.07008	0.06858	0.06728	0.00362
	0.035	0.05263	0.05061	0.05187	0.05170	0.00102
	0.04	0.05561	0.05431	0.05477	0.05490	0.00066
	0.05	0.05910	0.05613	0.05749	0.05757	0.00149
100	0	0.09601	0.09411	0.10243	0.09752	0.00436
	0.03	0.07248	0.07818	0.0749	0.07519	0.00286
	0.035	0.05495	0.05530	0.05565	0.05530	0.00035
	0.04	0.05742	0.06222	0.06424	0.06129	0.00350
	0.05	0.06405	0.06537	0.06595	0.06512	0.00097
150	0	0.09721	0.10414	0.10555	0.10230	0.00446
	0.03	0.07827	0.08466	0.08112	0.08135	0.00320
	0.035	0.06726	0.06852	0.06918	0.06832	0.00098
	0.04	0.06810	0.07198	0.07089	0.07032	0.00200
	0.05	0.06909	0.06781	0.06781	0.06824	0.00074
200	0	0.10927	0.11823	0.10941	0.11230	0.00513
	0.03	0.08701	0.08598	0.08841	0.08713	0.00122
	0.035	0.07164	0.07364	0.07213	0.07247	0.00104
	0.04	0.07537	0.07453	0.07249	0.07413	0.00148
	0.05	0.07653	0.07766	0.07615	0.07678	0.00079

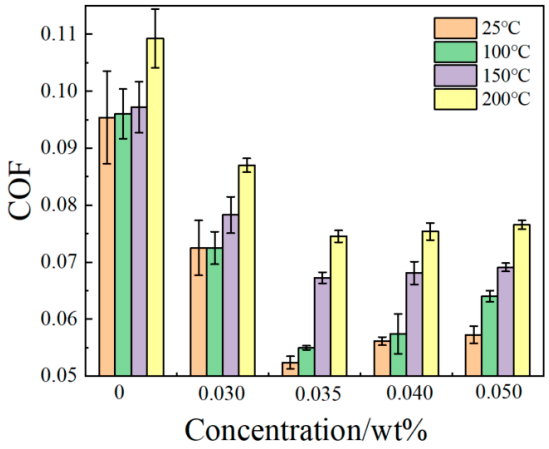

Figure 4. Average COFs with variation in temperature and concentrations.

4.2. Wear Properties

4.2.1. Surface Topography

After the tribological test, the wear extent of the upper steel ball is evaluated via SEM. The corresponding WSD is listed in Table 3 and plotted in Figure 5. It is notable that, although the WSD increases with temperature, the change in graphene concentration has little effect on the WSD at the same temperature. At 25 °C, the WSD of the steel ball surface with 0.035 wt% graphene lubricant is the lowest, which is 50.4% lower than that of the steel ball with pure oil.

Table 3. WSD under different conditions (μm).

Concentration/wt%	Temperature (°C)			
	25	**100**	**150**	**200**
0	835.22	1024.92	1050.06	1483.91
0.030	705.65	947.54	1109.02	1159.07
0.035	414.50	988.30	1094.76	1338.59
0.040	467.75	977.10	1131.56	1369.45
0.050	595.66	870.73	1114.49	1282.68

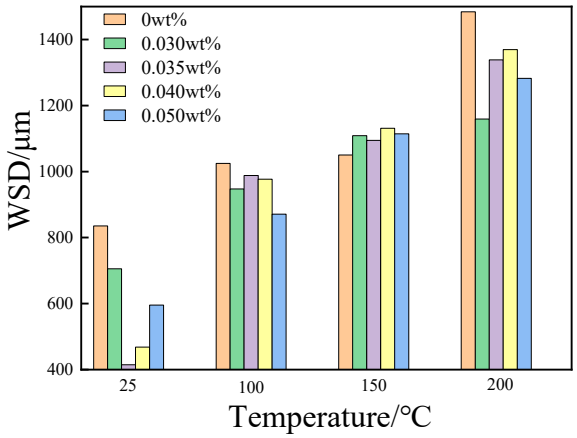

Figure 5. WSD under different conditions.

Figure 6 shows the wear morphology of the steel ball with different concentrations of graphene lubricant. It can be clearly seen in Figure 6a that the worn surface of the lubricant has many deep wear marks, and that the obvious grooves are large. After adding graphene, the WSD of the steel ball becomes smaller and the wear scar becomes shallower, contributing to a smoother surface. Accordingly, the worn surface is effectively separated by the friction reaction film during the friction process. The graphene lubricant film effectively inhibits the asperity summits shearing and the adhesive wear on the friction surface.

The transferred graphene particles are stacked on the surface, as shown by the red dashed circles in Figure 6b,c. There are two-body abrasive wear and three-body abrasive wear on the worn surfaces. In two-body wear, hard abrasive particles are fixed on the surface layer on one side of the friction pair. Furrowing occurs under the effect of shear force, and obvious scratches or grooves are produced on the worn surface. External abrasive particles move between the two friction surfaces. In three-body wear, hard abrasive particles are captured by two relatively moving surfaces, but they are still in a loose state. The damage is manifested by frictional irregular bite marks, pits, and a small amount of scratches and grooves on the subsurface.

Figure 7 depicts the morphology of adhesive wear on the steel surface when exposed to a high temperature. During the initial running-in process, the wear surface undergoes shear fracture, leading to the detachment of the sheared material and the formation of wear debris, resulting in adhesive wear. As the temperature increases, the width of the wear scar gradually expands, exacerbating the severity of wear. Specifically, at 200 °C as shown in Figure 7a, the wear scar exhibits a pronounced irregular shape, accompanied by the significant accumulation of graphene. When the COF is high and unstable, most of the graphene layers are worn or removed from the wear track, indicating the presence of graphite flakes near the track. This suggests that the graphene undergoes structural disorder due to modifications during the sliding process. The adhesion between surfaces leads to shear fracture and the subsequent detachment of material, giving rise to adhesive wear.

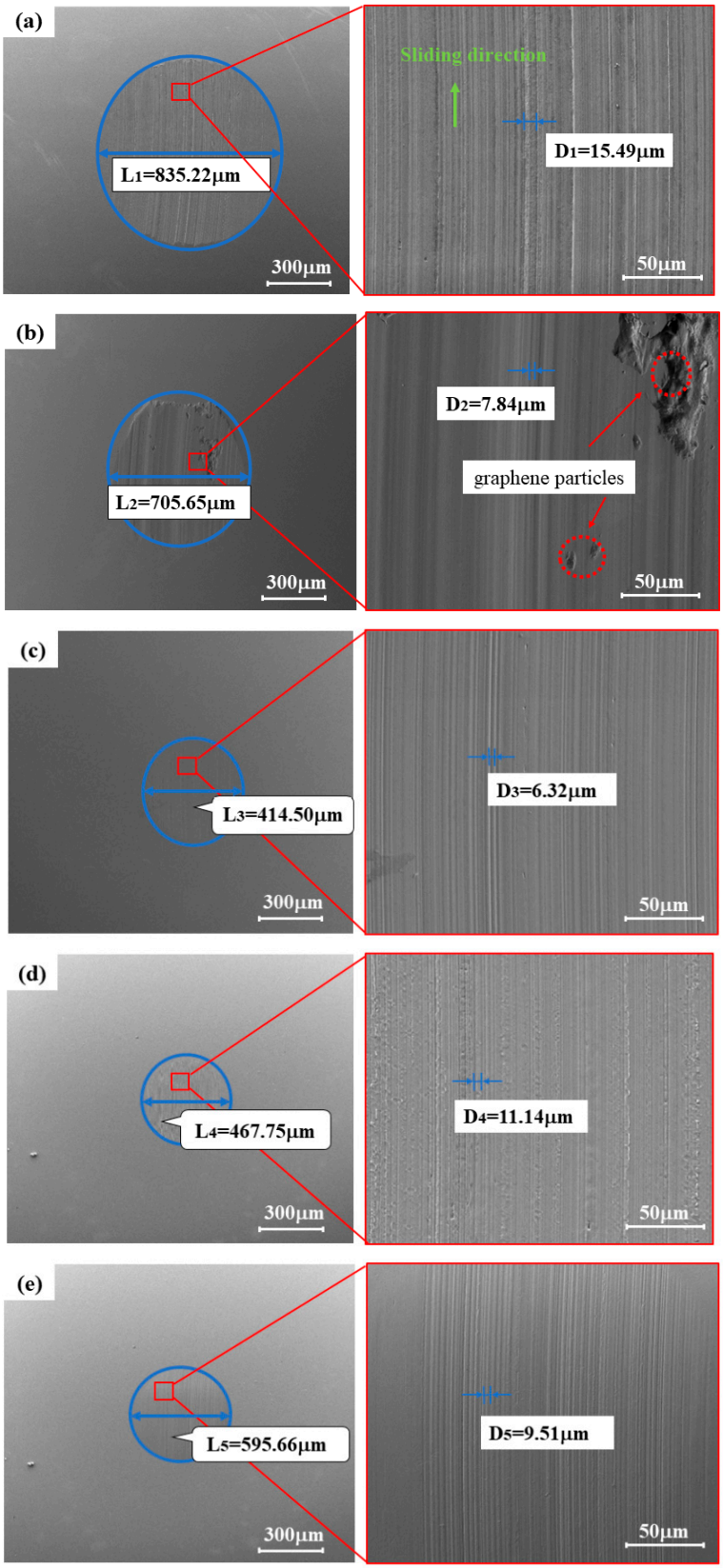

Figure 6. SEM images of a rigid ball with different graphene lubricants. (**a**) Pure oil; (**b**) 0.030 wt% graphene lubricant; (**c**) 0.035 wt% graphene lubricant; (**d**) 0.040 wt% graphene lubricant; (**e**) 0.050 wt% graphene lubricant.

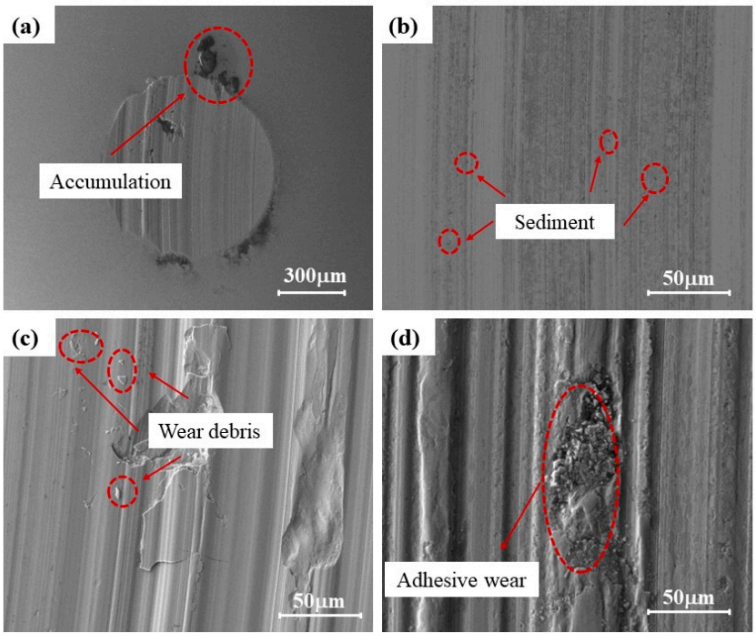

Figure 7. Adhesive wear surface morphology under a high temperature (200 °C): (**a**) Graphene accumulation, (**b**) Surface sediment, (**c**) Surface debris, (**d**) Adhesive wear.

The increase in temperature also causes a decline in the anti-wear and anti-friction properties of graphene lubricants and weakens their resistance to high temperatures. As the temperature increases, the oxidation reaction of the lubricant intensifies. Graphene plays a catalytic role in lubricating oil oxidation as a solid additive and accelerates its oxidation. Lubricants undergo polymerization and shear fragmentation with graphene that result in contamination and deterioration. This effect leads to an increase in lubricant viscosity, a decrease in the lubrication performance and severe wear. Consequently, the lubrication state between friction pairs evolves from elastohydrodynamic lubrication to mixed lubrication. Hence, it is imperative to enhance the high-temperature resistance of graphene lubricants.

In summary, the above analysis demonstrates that the thermal stability of the graphene oil film surpasses that of the base oil film, owing to the inhibited oxidation of graphite at high temperatures. This finding aligns with the exceptional tribological performance exhibited by the prepared coating under high-temperature conditions, as depicted in Figure 8. The energy spectrum of the worn surface when subjected to pure oil and graphene lubricating oil illustrates the effective integration of graphene into the friction interface, its ability to fill pits, and its wear-reducing properties.

As the temperature of the friction surface increases, the mechanical activation energy increases. As the local temperature and stress on the surface of the friction pair continue to increase, some nanoparticles firstly interact. The surface micro asperities of the friction pair produce nanometers and nanometers with a low COF, forming a chemical film with a low shear strength. In addition, nano-oxidation and slow oxidation form dense nano-films, whose COF is also very low. They form a chemical reaction film with nanometers and nanometers, and form an extreme pressure anti-wear repair layer together with the physical adsorption film, and the repair layer changes friction. The contact method of the secondary surface inhibits the furrowing, adhesion and fatigue wear of the friction pair surface, and improves the bearing capacity and anti-wear and anti-friction performance of the friction pair. Under higher loads, the friction pair is in a mixed lubrication state of fluid lubrication and boundary lubrication.

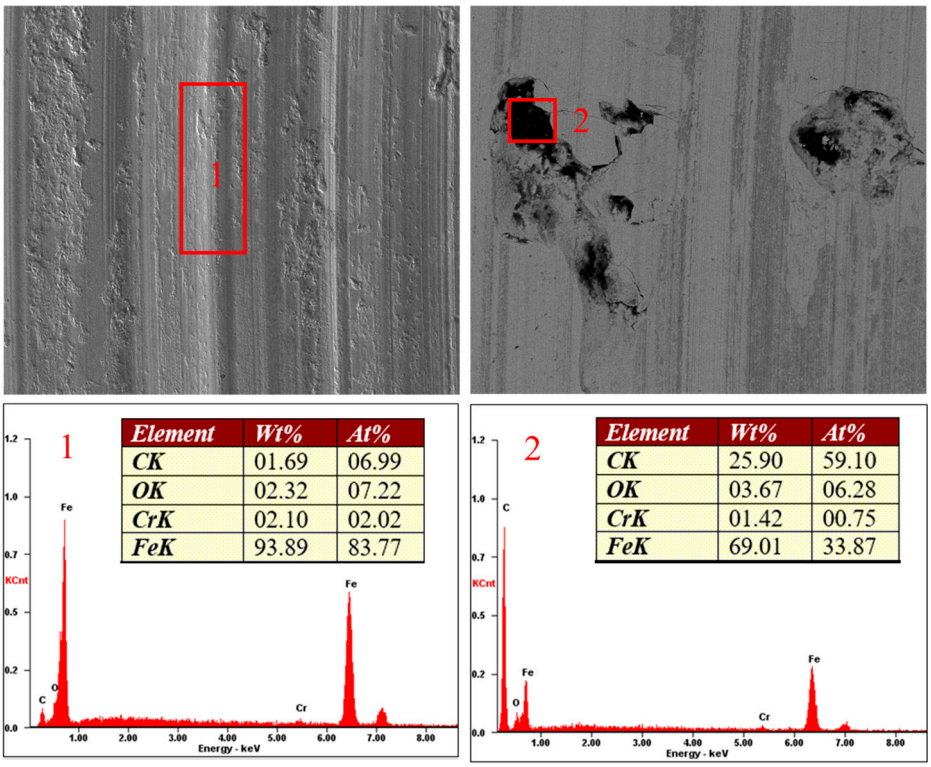

Figure 8. EDS of rigid sphere under the action of pure oil and graphene lubricants.

The addition of nanoparticles improves the anti-friction performance of the material, but does not improve the anti-wear performance of the material. This is because nanoparticles increase internal friction. In the later stage of violent friction, due to long-term friction, the increase in the surface temperature of the friction pair will reactivate the nanoparticles deposited on the wear marks and pits of the friction pair, and transfer to the surrounding environment along the surface with the friction. Under this action, the tribochemical reaction will eventually repair and smooth the worn surface.

Consequently, the increase in temperature leads to a gradual decrease in the anti-wear and anti-friction abilities of the graphene lubricant. Nevertheless, the graphene lubricant film still has a better thermal stability than the lubricant film, which is attributed to the oxidation inhibition of graphite at high temperatures. This is also consistent with the excellent tribological behavior of the as-prepared coatings at high temperatures.

4.2.2. The 3D Topography

To further compare the tribological properties of different concentrations of graphene lubricant at different temperatures, Figure 9 shows the three-dimensional image and surface roughness of the worn surface obtained using a white light interferometer. The wear depth data are shown in Figure 10. With the increase in the graphene concentration, the Ra and Rq of the worn surface first decrease and then increase, which is consistent with the change in WSD. As the surface roughness of the material increases, the contact area of the rough surface increases, leading to an increase in the COF. At different temperatures, the graphene lubricant has smaller wear marks (smaller wear volume and wear depth) than the pure oil. Adding the graphene, the morphology of the wear surface of the matrix changes obviously. Compared with pure oil, the addition of graphene can effectively reduce parallel grooves in the sliding direction, resulting in a smoother wear morphology. However, there are some gaps on the worn surface due to the abrasive wear effect of graphene as a hard particle.

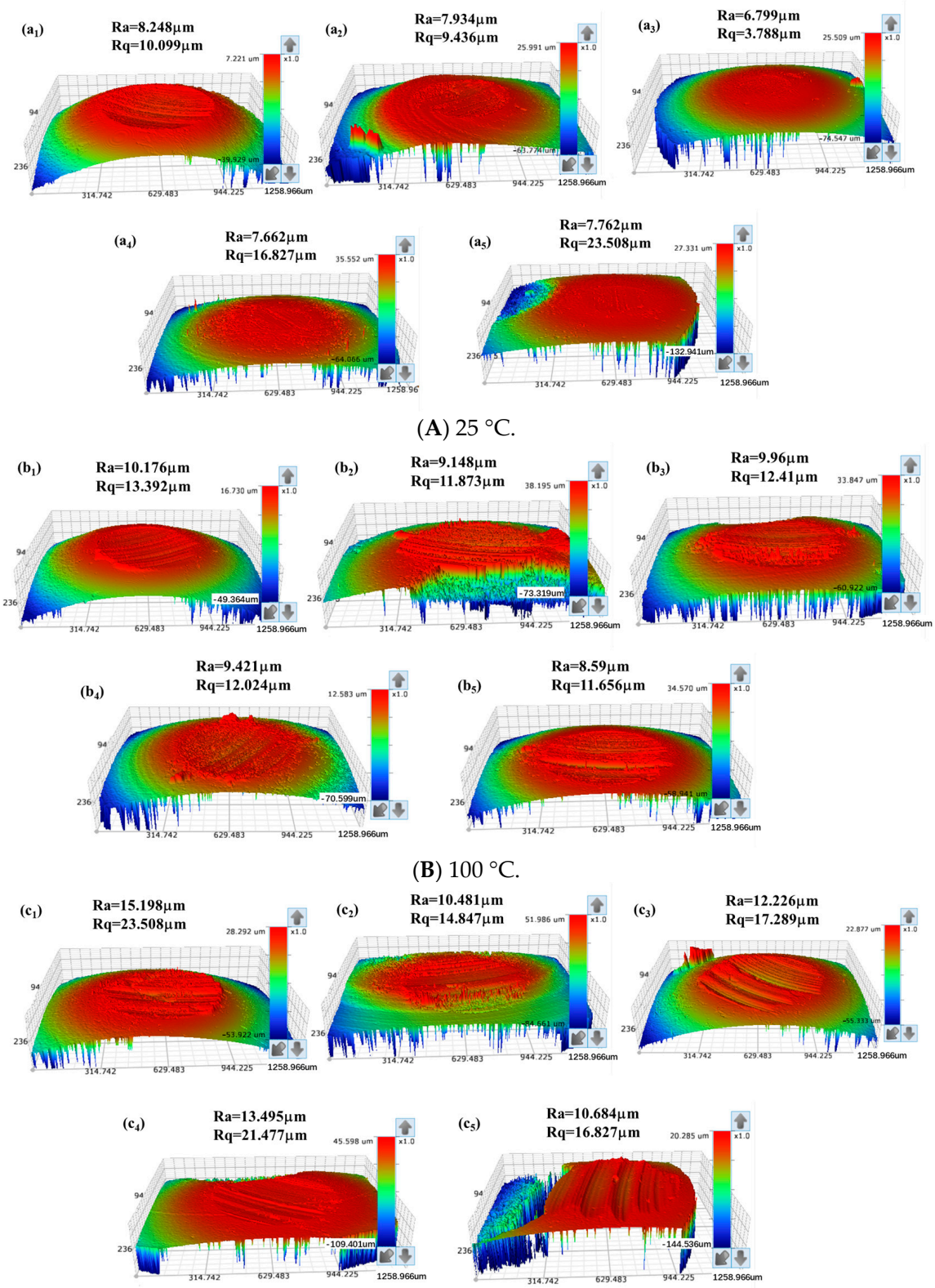

(**A**) 25 °C.

(**B**) 100 °C.

(**C**) 150 °C.

Figure 9. The 3D surface profiles and surface roughness with different graphene lubricants. (**A**) 25 °C, (**B**) 100 °C, (**C**) 150 °C.

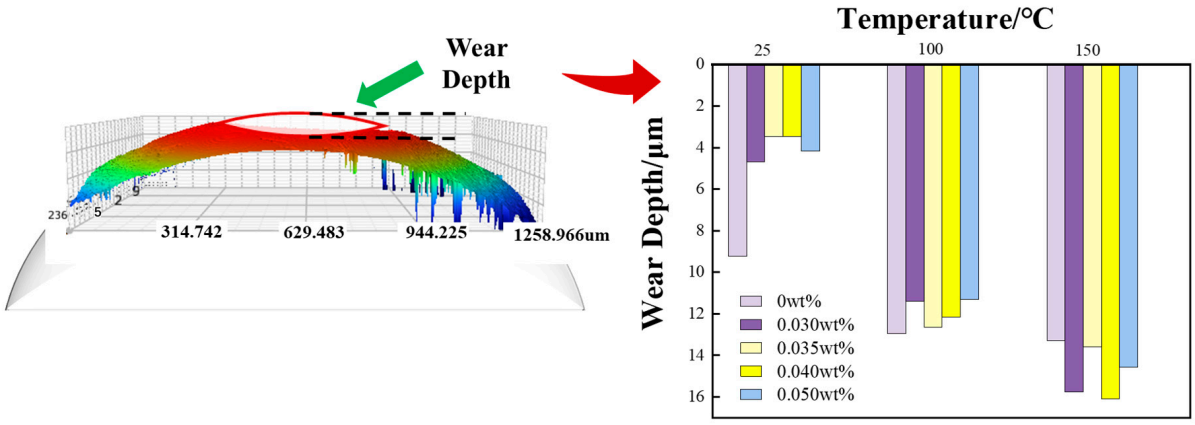

Figure 10. Surface wear depth with different graphene lubricants.

As the temperature increases, the number of asperities on the worn surface increases, and the morphology basically shows a sharp peak state. From Figure 10, it can be seen that, when the surface roughness is small, the local film thickness between the rough surfaces is thinner, and the fluid dynamic pressure is higher. The colors in the left figure represent the height of the ball, where red color represents the highest. Most of the normal loads are borne by the lubricating oil film, while the normal loads borne by the asperity are smaller. Therefore, the contact pressure of the asperity is lower, and the number of asperity contacts is smaller, as well as the actual contact area. Due to the small contact area of the asperity at this time, most of the friction heat is generated by the shear oil film. When the surface roughness is large, the local film thickness between rough surfaces increases, and the hydrodynamic pressure effect decreases. The normal load borne by the lubricating oil film decreases, while the normal load borne by the asperity increases. Therefore, the contact pressure of the asperity is higher, and the number of asperity contacts is larger, as well as the actual contact area. This is due to the high frictional heat generated by shear asperity contact at this moment.

4.3. Discussion

According to the experimental results of the COF and wear in Sections 3.1 and 3.2, the mechanisms can be assumed. Figure 11 shows a schematic drawing of the lubricating characteristics of graphene lubricants under different conditions, including the effects of graphene concentration and temperature. It is known that the microscopic topography of the contact surface consists of a large number of asperity summits and pits. On the surface of the asperity summits, the graphene particles and polar molecules in the lubricant act together as a physical adsorption film. At the onset of friction, since the density of the particles is larger than that of the lubricant, homogeneously dispersed graphene particles are rapidly deposited in the pits under the action of hydrodynamic pressure. When the mass fraction of graphene increases, the COF tends to be stable; this is because the lubricant film formed is sufficient to withstand the shear stress under the test conditions. When the graphene lubricant concentration continues to increase, it causes graphene to accumulate on the surface of the friction pair, so that the oil film of the lubricant cannot be formed normally, resulting in an increase in the COF. Therefore, further increasing the additive amount will not further improve the tribological properties. This could be the reason that the graphene lubricant with a 0.035% concentration has a good performance regarding the tested steel–steel friction pairs.

Graphene nanoparticles and fine iron abrasive particles will drop into the wear scars and fill the pits after lubrication to reduce wear. After adding a certain amount of graphene to the base oil, the oil film can still play an important role in the friction and wear process. At low concentrations, graphene particles play a certain lubricating role and can repair rough surfaces. At an appropriate concentration, the graphene particles have the best lubricating

effect, and the rough surface can be repaired to be smoother. However, graphene particles at high concentrations will agglomerate in a large area, and the agglomerated particles will act as wear debris to intensify wear.

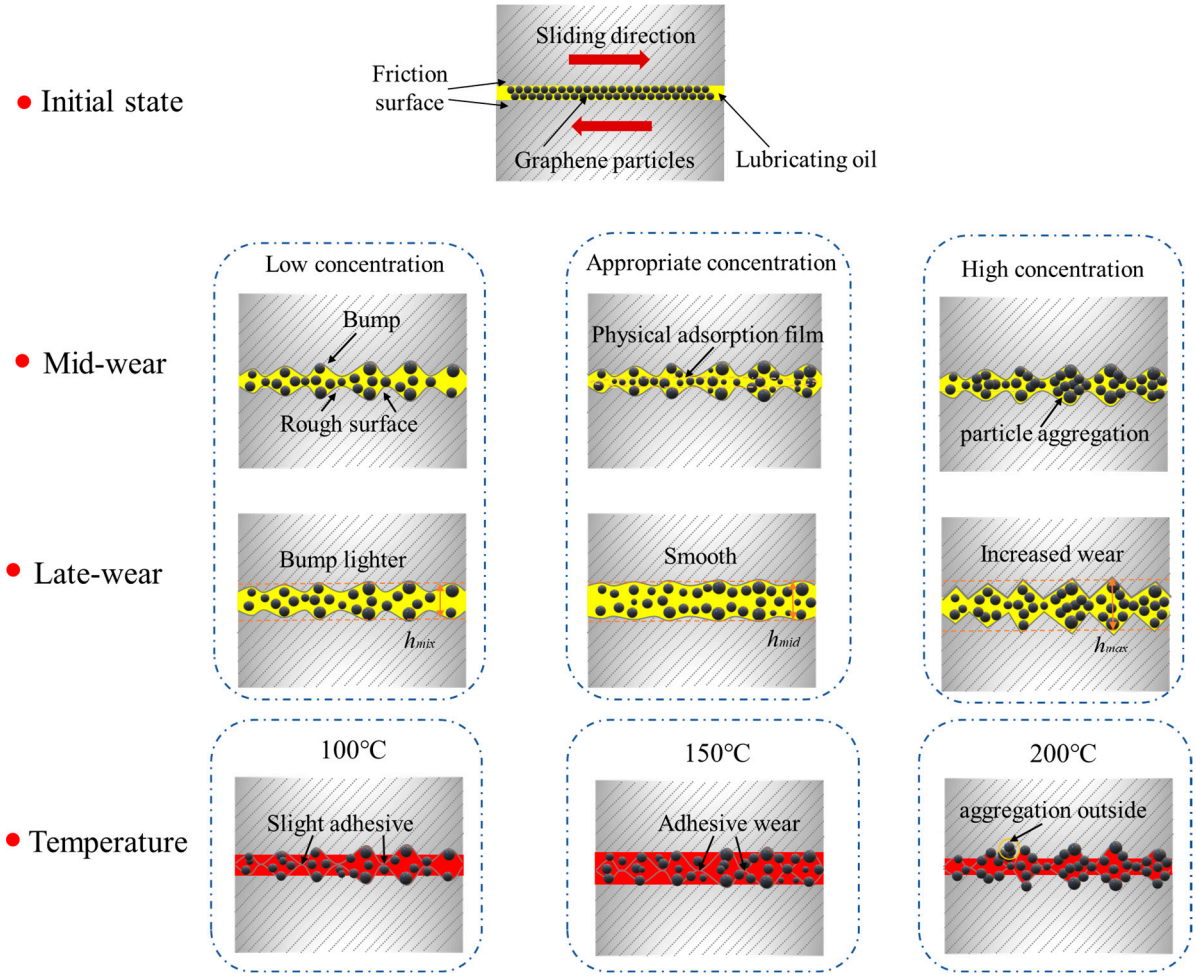

Figure 11. Schematic drawing of graphene lubricant under different conditions.

The effect of temperature on the friction performance is the change in the lubrication state, from hydrodynamic lubrication to boundary lubrication and even dry friction. This causes changes in the surface structure during the friction process; that is, there are friction changes between the friction surface and the surrounding medium, such as diffusion, adsorption or desorption between surface atoms or molecules, surface structure changes and phase transitions. The phenomenon in Figure 3d is caused by the increase in the thermal motion of atoms with increased temperature, resulting in a transition of the lubricating state. The transformation from hydrodynamic lubrication to boundary lubrication or even dry friction causes changes in the surface layer structure during the friction process. Additionally, with the increase in temperature, the adhesive wear of the worn surface intensifies, and some graphene particles agglomerate around the wear scar.

5. Conclusions

The results of the friction and wear experiments show that graphene lubricants have excellent anti-wear and anti-friction abilities. Compared with the pure oil, the COF and WSD of steel balls under the 0.035 wt% graphene lubricant decreased by 40.8% and 50.4%. After micro three-dimensional surface analysis, the lubrication characteristics were attributed to the synergistic effect of graphene particles on the wear surface to protect and repair the friction surface. The adsorbed lubricating film inhibits furrowing, adhesion,

and fatigue wear on the friction pair's surface, improving the bearing capacity, as well as the anti-wear and friction-reducing effects. It shows that graphene has broad application prospects as a lubricant additive.

Author Contributions: Conceptualization, Y.D. and Y.L.; methodology, Y.D.; software, Q.Z.; validation, Y.D., C.X. and Y.L.; formal analysis, Y.D.; investigation, Y.D.; resources, B.M. and C.X.; data curation, Y.D.; writing—original draft preparation, Y.D.; writing—review and editing, C.X.; visualization, Y.D.; supervision, B.M. and C.X.; project administration, B.M. and C.X.; funding acquisition, B.M. and C.X. All authors have read and agreed to the published version of the manuscript.

Funding: This research was funded by the National Natural Science Foundations of China, grant number [52175037 and 51805289] and the APC was funded by [51805289].

Data Availability Statement: Data are contained within the article.

Conflicts of Interest: The authors declare no conflict of interest.

References

1. Zhao, J.; Huang, Y.; He, Y.; Shi, Y. Nanolubricant additives: A review. *Friction* **2021**, *9*, 891–917. [CrossRef]
2. Li, Y.; Yang, R.; Hao, Q.; Lei, W. Tribological Properties of the Functionalized Graphene/Montmorillonite Nanosheets as a Lubricant Additive. *Tribol. Lett.* **2021**, *69*, 117. [CrossRef]
3. Cyriac, F.; Yi, T.X.; Poornachary, S.K.; Chow, P.S. Boundary lubrication performance of polymeric and organic friction modifiers in the presence of an anti-wear additive. *Tribol. Int.* **2022**, *165*, 107256. [CrossRef]
4. Yin, Y.; Lei, H.; Song, J.; Zhao, G.; Ding, Q. Molecular Dynamics Simulation on the Tribological Properties of Polytetrafluoroethylene Reinforced with Modified Graphene. *Tribology* **2022**, *42*, 598–608. [CrossRef]
5. Zhao, X.; Tian, C.; Hao, L.; Xu, H.; Dong, J. Tribology and Rheology of Polypropylene Grease with MoS_2 and ZDDP Additives at Low Temperatures. *Lubricants* **2023**, *11*, 464. [CrossRef]
6. Ali, M.K.A.; Hou, X. Exploring the lubrication mechanism of CeO_2 nanoparticles dispersed in engine oil by bis(2-ethylhexyl) phosphate as a novel anti-wear additive. *Tribol. Int.* **2022**, *165*, 107321. [CrossRef]
7. Ares, P.; Novoselov, K.S. Recent advances in graphene and other 2D materials. *Nano Mater. Sci.* **2022**, *4*, 3–9. [CrossRef]
8. Li, Z.; Gao, C.; Zhao, H. Porous biomass-derived carbon modified by Cu, N co-doping and Cu nanoparticles as high-efficient electrocatalyst for oxygen reduction reaction and zinc-air battery. *J. Alloys Compd. Interdiscip. J. Mater. Sci. Solid-State Chem. Phys.* **2022**, *897*, 163175. [CrossRef]
9. Zhang, K.Y.; Yin, Y.G.; Zhang, G.T.; Ding, S.G.; Chen, Q. Tribological Properties of FeS/Cu Copper-Based Self Lubricating Bearing Materials Prepared by Mechanical Alloying. *Tribol. Trans.* **2020**, *63*, 197–204. [CrossRef]
10. Hu, Z.; Chen, J.; Pan, P.; Liu, C.; Zeng, J.; Ou, Y.; Qi, X.; Liang, T. Porous N-doped Mo_2C@C nanoparticles for high-performance hydrogen evolution reaction. *Int. J. Hydrogen Energy* **2022**, *47*, 4641–4652. [CrossRef]
11. Huai, W.J.; Zhang, C.H.; Wen, S.Z. Graphite-based solid lubricant for high-temperature lubrication. *Friction* **2021**, *9*, 1660–1672. [CrossRef]
12. Jamel, R.S.; Al-Murad, M.A.; Alkhalidi, E.F. The efficacy of reinforcement of glass fibers and ZrO_2 nanoparticles on the mechanical properties of autopolymerizing provisional restorations (PMMA). *Saudi Dent. J.* **2023**, *35*, 707–713. [CrossRef]
13. Qi, H.; Zhang, G.; Zheng, Z.; Yu, J.; Hu, C. Tribological properties of polyimide composites reinforced with fibers rubbing against Al_2O_3. *Friction* **2020**, *9*, 301–314. [CrossRef]
14. Wang, F.J. Spherical-shaped CuS modified carbon nitride nanosheet for efficient capture of elemental mercury from flue gas at low temperature. *J. Hazard. Mater.* **2021**, *415*, 125692. [CrossRef]
15. Qian, Y.T. Facile synthesis of sub-10 nm ZnS/ZnO nanoflakes for high-performance flexible triboelectric nanogenerators. *Nano Energy* **2021**, *88*, 106256. [CrossRef]
16. Soetaredjo, F.E.; Santoso, S.P.; Waworuntu, G.; Darsono, F.L. Cellulose Nanocrystal (CNC) Capsules from Oil Palm Empty Fruit Bunches (OPEFB). *Biointerface Res. Appl. Chem.* **2022**, *12*, 2013–2021. [CrossRef]
17. Liu, J.P.; Zhang, H.R.; Yan, Q.L. Anti-sintering behavior and combustion process of aluminum nano particles coated with PTFE:A molecular dynamics study. *Def. Technol.* **2023**, *24*, 46–57. [CrossRef]
18. Su, Y.; Li, Y.F.; Gong, S.G.; Song, Y.H.; Li, B.; Wu, X.L.; Zhang, J.P.; Liu, D.T.; Shao, C.L.; Sun, H.Z. Graphene wrapped TiO_2@$MoSe_2$ nano-microspheres with sandwich structure for high-performance sodium-ion hybrid capacitor. *Appl. Surf. Sci. J. Devoted Prop. Interfaces Relat. Synth. Behav. Mater.* **2023**, *610*, 155494. [CrossRef]
19. Wang, G.; Liu, X.B.; Zhu, G.X.; Zhu, Y.; Liu, Y.F.; Zhang, L.; Wang, J.L. Tribological study of Ti_3SiC_2/Cu_5Si/TiC reinforced Co-based coatings on SUS304 steel by laser cladding. *Surf. Coat. Technol.* **2022**, *432*, 128064. [CrossRef]
20. Liu, L.; Zhou, M.; Mo, Y.; Bai, P.; Wei, Q.; Jin, L.; You, S.; Wang, M.; Li, L.; Chen, X.; et al. Synergistic lubricating effect of graphene/ionic liquid composite material used as an additive. *Friction* **2021**, *9*, 1568–1579. [CrossRef]
21. Kaleli, E.H.; Demirtas, S. Experimental investigation of the effect of tribological performance of reduced graphene oxide additive added into engine oil on gasoline engine wear. *Lubr. Sci.* **2023**, *35*, 118–143. [CrossRef]

22. Sun, S.; Ru, G.; Qi, W.; Liu, W. Molecular dynamics study of the robust superlubricity in penta-graphene van der Waals layered structures. *Tribol. Int.* **2023**, *177*, 107988. [CrossRef]
23. Zhang, Y.; Tai, X.; Zhou, J.; Zhai, T.; Xu, L.; Diao, C.; Xie, X.; Hou, C.; Sun, X.; Zhang, X.; et al. Enhanced high-temperature thermal conductivity of the reduced graphene oxide@SiO_2 composites synthesised by liquid phase deposition. *Ceram. Int.* **2022**, *48*, 8481–8488. [CrossRef]
24. Wang, H.; Bai, Q.; Chen, S.; Dou, Y.; Guo, W. Nanoscale mechanism of suppression of friction and wear of the diamond substrate by graphene. *Mater. Today Commun.* **2022**, *33*, 104894. [CrossRef]
25. Chen, G.Y.; Zhao, J.; He, Y.Y.; Luo, J.B. Synthesis and Structure Control of Graphene Lubricant Additives. *Tribology* **2021**, *41*, 758–772. [CrossRef]
26. Saufi, M.A.; Mamat, H. Comparison of dispersion techniques of graphene nanoparticles in polyester oil. *Mater. Today Proc.* **2022**, *66*, 2747–2751. [CrossRef]
27. Sarath, P.S.; Reghunath, R.; Thomas, S.; Haponiuk, J.T.; George, S.C. An investigation on the tribological and mechanical properties of silicone rubber/graphite composites. *J. Compos. Mater.* **2021**, *55*, 002199832110316. [CrossRef]
28. Ci, X.; Zhao, W.; Luo, J.; Wu, Y.; Ge, T.; Xue, Q.; Gao, X.; Fang, Z. How the fluorographene replaced graphene as nanoadditive for improving tribological performances of GTL-8 based lubricant oil. *Tribology* **2021**, *9*, 488–501. [CrossRef]
29. Lau, G.A.; Neves, G.O.; Salvaro, D.B.; Binder, C.; Klein, A.N.; de Mello, J.D. Stability and Tribological Performance of Nanostructured 2D Turbostratic Graphite and Functionalised Graphene as Low-Viscosity Oil Additives. *Lubricants* **2023**, *11*, 155. [CrossRef]
30. Zhang, C.; Zhang, X.; Zhang, W.; Zhao, Z.; Fan, X. Functionalized Graphene from Electrochemical Exfoliation of Graphite toward Improving Lubrication Function of Base Oil. *Lubricants* **2023**, *11*, 166. [CrossRef]
31. Liu, Y.; Dong, Y.; Zhang, Y.; Liu, S.; Bai, Y. Effect of different preparation processes on tribological properties of graphene. *Nanomater. Nanotechnol.* **2020**, *10*, 184798042094665. [CrossRef]
32. Jiang, Z.; Yang, G.; Zhang, Y.; Gao, C.; Ma, J.; Zhang, S.; Zhang, P. Facile method preparation of oil-soluble tungsten disulfide nanosheets and their tribological properties over a wide temperature range. *Tribol. Int.* **2019**, *135*, 287–295. [CrossRef]
33. Han, Z.; Gan, C.; Li, X.; Feng, P.; Ma, X.; Fan, X.; Zhu, M. Electrochemical preparation of modified-graphene additive towards lubrication requirement. *Tribol. Int.* **2021**, *161*, 107057. [CrossRef]